Check for updates

Silver-coated eggshell membrane as a cost-effective SERS platform for enhanced molecular sensing†

V.S. Swathy Lekshmy, [ab] Subramee Sarkar,‡[a] Karuvath Yoosaf,§[a] Joshy Joseph [iD] *[ab] and P. Sujatha Devi [iD] *[ab]

Surface-enhanced Raman spectroscopy (SERS) is a surface-sensitive analytical technique that relies heavily on plasmonic substrates to enhance Raman scattering. In this study, we report the fabrication of a cost-effective SERS substrate by thermally evaporating silver (Ag) onto the eggshell membrane (ESM), a low-cost and biologically sourced material, to create substrates with controlled surface morphologies. The silver coating thickness has been varied to optimize the signal enhancement and was evaluated with three different standard Raman active molecules: 4-mercaptobenzoic acid (4-MBA), 4-mercaptophenylboronic acid (4-MPBA), and rhodamine 6G (R6G)- as analytes. The developed substrates exhibited remarkable SERS activity with an Enhancement Factor (EF) of 0.12×10^6 for 4-MBA, 0.70×10^5 for 4-MPBA and 0.36×10^4 for R6G, respectively. The ESM with optimal silver deposition of a thickness of 20 nm exhibited significantly enhanced SERS signal, with improved sensitivity and detection limit for all the three molecular analytes. Present study also highlights the importance of precise control over the metal coating thickness on ESM by thermal evaporation to achieve optimal SERS performance. Notable contribution is the fabrication of silver-coated eggshell membrane (ESM/Ag) as a cost-effective promising SERS platform for high-performance molecular sensing applications.

1. Introduction

Surface-enhanced Raman spectroscopy (SERS) is a powerful vibrational analytical tool that has been actively researched for the past few decades. It is used in various fields such as sensing, medicine, catalysis, food safety assessment, environmental monitoring, and so on.[1] SERS surpasses conventional Raman spectroscopy by amplifying the Raman scattering to a factor of 10^8 or even higher *via* probing the inelastically scattered light by molecules adsorbed on a plasmonic nanometallic surface.[2]

The substantial improvement in the Raman signal intensity can be explained by the electromagnetic enhancement mechanism emanating from surface plasmon excitation in metal nanoparticles functioning as the SERS substrate and the chemical enhancement mechanism associated with charge transfer between the analyte molecule and the substrate.[3] SERS

[a] Chemical Sciences and Technology Division, CSIR-National Institute for Interdisciplinary Science and Technology, Thiruvananthapuram-695019, Kerala, India. E-mail: psujathadeviniist@gmail.com; psujathadevi@gmail.com

[b] Academy of Scientific and Innovative Research (AcSIR), Ghaziabad-201002, India

† Electronic supplementary information (ESI) available. See DOI: https://doi.org/10.1039/d5ra02461g

‡ Current affiliation: Centre for Analysis and Synthesis, Department of Chemistry, Lund University, P. O. Box 124, SE-22100 Lund, Sweden.

§ Current affiliation: Department of Applied Chemistry, Cochin University of Science and Technology, Kochi 682022, Kerala, India.

is a versatile technique that demands highly reliable substrates in terms of sensitivity, reproducibility, stability, and cost-effectiveness. The 'reliability' is determined greatly by the type of substrate material used and the fabrication method. Typical SERS-active platforms include nanostructures on glass,[4] quartz,[5] or highly ordered nanostructures fabricated through nanolithography,[6] chemical etching,[7] *etc.* However, these substrates are often expensive and rigid, making them unsuitable for real-life applications. Therefore, researchers are now focusing on using flexible, inexpensive and environmentally acceptable substrates for SERS. Bio-templates like rose petals,[8,9] butterfly wings,[10,11] and cicada wings[12] have been successfully employed in fabricating SERS substrate.

Eggshell membrane (ESM) is a unique biomaterial rich in amino acids like glycine and alanine, uronic acid, collagen (types I, V and X), and other proteins.[13,14] It is often discarded as waste but can be used as a template for creating various useful materials.[15–17] ESMs are employed in the synthesis of nanoparticles,[15] recovery of heavy metals,[18,19] dyes,[20] and enzyme immobilized bio-sensing applications.[21,22] However, there has been very few studies on ESM-templated SERS substrates. Lin *et al.*[23] fabricated a three-dimensional (3D) SERS platform of porous ESM scaffold decorated with Ag nanoparticles (AgNPs) by *in situ* reduction of silver nitrate with ascorbic acid. It is reported that by controlling the porosity of the ESM membrane through H_2O_2 treatment, there was an improvement in SERS

enhancement. This was due to the densely packed AgNPs on the treated ESM fibers. Another study reported the *in situ* SERS monitoring of catalytic reactions achieved by assembling Ag nanoprisms on ESM.[24] Researchers have also developed an ESM-templated substrate *via* the *in situ* deposition of gold nanoparticles on ESM to detect the pesticide thiabendazole with a detection limit of 0.1 ppm.[25] Similarly, an *in situ* reduction strategy for immobilizing nanoparticles on ESM was employed for SERS detection of antibiotic spiramycin in aqueous samples.[26] All the studies on the ESM SERS substrate reported so far have proposed the fabrication by depositing a preformed nanoparticle colloid or its precursor solution onto the membrane.

This study reports the fabrication of a three-dimensional, flexible SERS platform based on Ag-immobilized ESM (ESM/Ag) using the thermal evaporation technique for molecular detection. Thermal evaporation offers several significant advantages over traditional solution-based methods. It allows for precise control over the amount, thickness, and uniformity of the deposited metal, which is crucial for consistently generating SERS-active hotspots.[27] Additionally, thermal evaporation is a clean, solvent-free process that eliminates the need for chemical reducing agents or surfactants, thereby enhancing the purity and stability of the final substrate. To the best of our knowledge, this is the first report that investigates the use of thermal evaporation for the preparation of ESM-based substrates. The resulting platform combines the intrinsic porosity and flexibility of ESM with SERS properties of thermally deposited silver to create a cost-effective, scalable, and highly sensitive SERS substrate. The fabrication method, structural and morphological characterization, and SERS performance of the ESM/Ag substrate using standard analytes are systematically presented and discussed in this study.

The analytes chosen for this study—4-mercaptobenzoic acid (4-MBA), 4-mercaptophenylboronic acid (4-MPBA), and rhodamine 6G (R6G)—serve as model compounds with significant relevance in various sensing applications. 4-MBA is widely used as a Raman reporter due to its strong affinity for noble metal surfaces and its well-defined vibrational features, making it valuable for biosensing and characterizing nanoparticle surfaces.[28] 4-MPBA, featuring a boronic acid functional group, is important for detecting diol-containing biomolecules like glucose, positioning it as a crucial probe in medical diagnostics and biochemical assays.[29] R6G, a commonly used dye, is often employed in environmental monitoring and SERS calibration due to its strong Raman scattering cross-section and well-characterized spectral behavior.[30] The ability to detect these analytes sensitively and reproducibly not only validates the performance of the ESM/Ag SERS substrate but also highlights its potential for practical applications in biomedical, environmental, and analytical chemistry fields.

2. Experimental procedure

2.1 Fabrication of ESM/Ag substrates

Cleaned chicken eggshells were soaked in dilute acetic acid for 15–30 minutes. The eggshell membranes were then carefully extracted and thoroughly washed with distilled water to remove albumen and then air dried. Once dried, the membranes were cut into uniform pieces and securely mounted onto a glass slide for uniform Ag coating during the thermal evaporation process by using Smart Coat 3.0 thermal evaporator, Hind High Vacuum Company Pvt. Ltd, India. The silver was evaporated at a rate of 0.5 Å s^{-1} while enabling substrate rotation ($\sim$8 rpm). The rate was monitored using a quartz crystal microbalance for real-time measurement of the deposition thickness. ESM substrates with different Ag coating thicknesses, ESM/xAg, were fabricated, where x denotes the Ag coating thickness in nanometer.

2.2 Characterization

The morphological features of ESM and silver coated ESM were observed using Carl Zeiss-Sigma Field Emission Scanning Electron Microscope (FESEM) and Bruker Multimode 8 Atomic Force Microscope (AFM) operating in tapping mode. X-ray diffraction (XRD) studies were conducted using a powder X-ray diffractometer, Malvern Panalytical, UK. X-ray photoelectron spectroscopy (XPS) was conducted on a PHI 5000 VersaProbe II instrument, ULVAC-PHI Inc., USA, equipped with micro-focused (200 μm, 15 kV) monochromatic Al-Kα X-ray source ($h\nu$ = 1486.6 eV). Data was calibrated against C 1s (binding energy, 284.8 eV). XPS data were processed using PHI's Multipak software.

2.3 SERS measurements

The Raman active molecules, 4-MBA (4-mercaptobenzoic acid), 4-MPBA (4-Mercaptophenylboronic acid) and R6G (Rhodamine 6G) used for the experiments were purchased from Sigma Aldrich Chemicals Pvt. Ltd, USA. All the analyte solutions were prepared in analytical grade ethanol (SpectroChem Pvt. Ltd, India). 20 μL of the analyte solutions were drop cast onto 0.5 cm × 0.5 cm of the SERS substrate and air dried before data acquisition. Raman measurements were carried out using a Mira DS handheld Raman spectrometer (Ms. Metrohm India Ltd – Mira Cal DS software) with an excitation wavelength of 785 nm. The spectrometer works in the spectral range 400–2300 cm^{-1} with a resolution of $\sim$10 cm^{-1}. The raw spectra acquired were processed for background removal and baseline correction using Savitzky–Golay Coupled Advanced Rolling Circle Filter (SCARF), a method developed by T. M. James *et al.*[31] The overall data analysis was carried out on custom-written software in the LabVIEW programming environment.

3. Results and discussion

3.1 Fabrication of ESM/Ag substrates

The SERS substrates were fabricated by depositing silver onto the surface of ESM using a thermal evaporation method. ESM substrates with varying thicknesses of silver coating, represented as ESM/xAg (where x = 5, 10, 20, 40, 60, 80, 100 nm) were generated at an evaporation rate of 0.5 Å s^{-1}. A schematic illustration of the entire fabrication process is provided in Fig. 1.
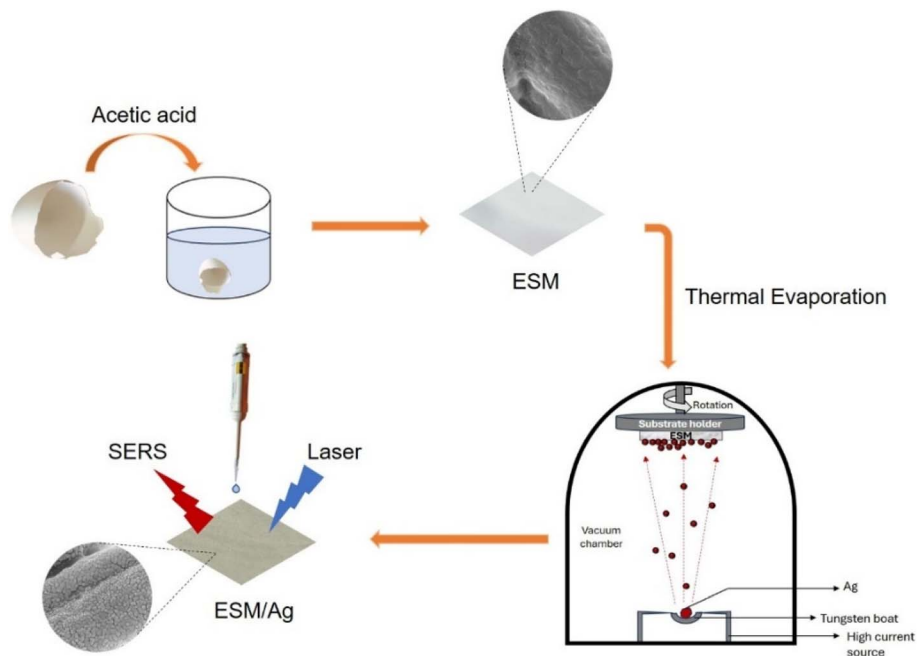
Fig. 1 Schematic illustration of the fabrication process for silver-coated ESM substrates.

3.2 ESM/Ag substrate characterization

The XRD patterns of natural ESM and ESM/Ag substrates are shown in Fig. 2. The natural ESM shows an amorphous character. However, after silver coating, the ESM/20Ag substrate exhibited a diffraction peak at $2\theta = 38.32°$ corresponding to Ag (111) crystal plane. As the Ag thickness increased, additional diffraction peaks appeared at 44.21°, 64.44°, 77.36°, and 81.48°, which can be indexed to (200), (220), (311), and (222) planes of silver, respectively (JCPDS No. 01-087-0597). This confirms that the Ag layer on the membrane was predominantly in its metallic state and did not oxidize under the deposition conditions used in this study.

High-resolution XPS spectra of the Ag 3d region confirms the chemical state of Ag on the ESM surface (Fig. 3). The analysis shows two peaks at 368.4 eV and 374.4 eV, corresponding to Ag $3d_{5/2}$ and $3d_{3/2}$ binding energies, respectively. These results further indicate that the silver is deposited on the surface of ESM as metallic Ag.[32]
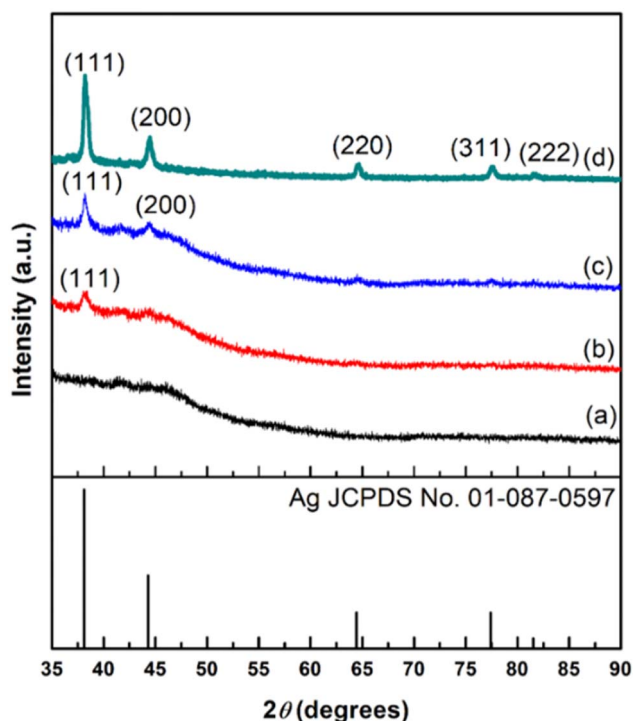

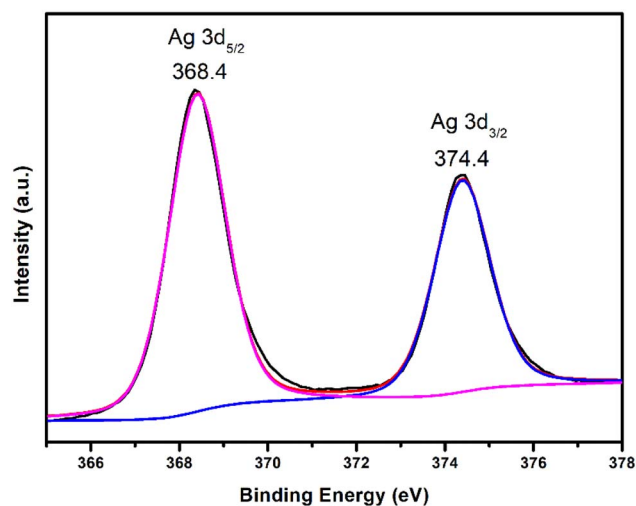Fig. 2 XRD patterns of (a) ESM, (b) ESM/20Ag (c) ESM/40Ag and (d) ESM/100Ag.

Fig. 3 XPS spectra of ESM/20Ag depicting the zero valent Ag 3d spectra.

The deposition of Ag on the ESM can also be observed from the change in the colour of the membrane from white (bare ESM) to yellow for 5 nm, dark grey for 20 nm Ag coating, and silvery for higher coating thicknesses as shown in Fig. 4a–e.

A clear insight into the distribution of Ag on the membrane was achieved through FE-SEM images shown in Fig. 4f–o. As reported earlier, the natural ESM had a 3D network structure consisting of interwoven fibers and pores which is evident here in Fig. 4f.[15] After the Ag deposition, the ESM substrate retained its 3D network structure, with Ag deposited on the fibrous structure of ESM (Fig. 4g–j). This characteristic is essential for preserving the functional integrity of the substrate, making it suitable for potential applications in biosensing and chemical sensing. It is observed that the thickness of the silver coating significantly impacts the surface morphology. The deposition of Ag on ESM exhibited characteristics consistent with Volmer–Weber growth. At low coating thicknesses, such as 5 nm, the silver particles are smaller and randomly distributed, with noticeable gaps between them (Fig. 4l). As a result, the film has less coverage, exposing areas of the membrane fibers. As the coating thickness has increased to 20 nm, the silver layer appeared more continuous, albeit with small gaps, producing island-like nanostructures on the surface (Fig. 4m). These gaps are significant for SERS, as the nanogaps between islands may create hot spots where the electromagnetic field is highly localized and enhanced.[33] As the Ag thickness increased further, the gaps were progressively filled, covering the ESM fibers. At higher thicknesses, such as 100 nm, the silver layer forms a relatively continuous, smooth film (Fig. 4o). However, this can result in lower signal enhancement due to reduced hotspots.

3.3 Evaluation of SERS performance of ESM/Ag with Raman standards

In order to investigate the influence of Ag coating thicknesses, spectra of commonly used Raman reporter molecules, namely 4-MBA, 4-MPBA, and R6G, were measured for substrates with different coating thicknesses *i.e.* 5, 10, 20, 40, 60, 80 and 100 nm. The major peaks of 4-MBA on the ESM/Ag substrate were found to be centered at 1585 cm^{-1} (aromatic ring breathing mode), 1422 cm^{-1} (symmetric stretching vibration of carboxylate group), 1185 cm^{-1} (C–H deformation mode), 1078 cm^{-1} (aromatic ring vibration possessing C–S stretching mode) (Fig. 5a). The SERS peaks for 4-MPBA were observed at 1585 cm^{-1} (C–C ring breathing mode), 1188 cm^{-1} (in-plane C–H bending), 1072 cm^{-1} (in-plane benzene ring breathing mode coupled with C–S stretching mode), 469 cm^{-1} (out-of-plane ring vibration) (Fig. 5b). The Raman peaks obtained for both 4-MBA and 4-MPBA on ESM/Ag were similar to those observed in the earlier works.[34,35] Peaks observed for R6G at 1650, 1509, 1363 and 1311 cm^{-1} can be assigned to aromatic CC stretching, at 773 cm^{-1} for C–H out-of-plane bending, and 614 cm^{-1} corresponding to CCC ring in-plane bending (Fig. 5c), are also in agreement with the previously reported studies.[36] Fig. 6a–c show the intensities of the characteristic peaks of 4-MBA (1078 and 1585 cm^{-1}), 4-MPBA (1072 and 1585 cm^{-1}) and R6G (1311, 1363 and 1509 cm^{-1}) respectively, against varying Ag coating thickness. It is observed that the intensities of these peaks increase with an increase in Ag coating thickness, attain a maximum value for ESM substrate coated with 20 nm Ag, and further decrease. Therefore, all the further SERS studies were conducted using ESM with a silver coating thickness of 20 nm. The FE-SEM images corroborate the comparatively superior SERS
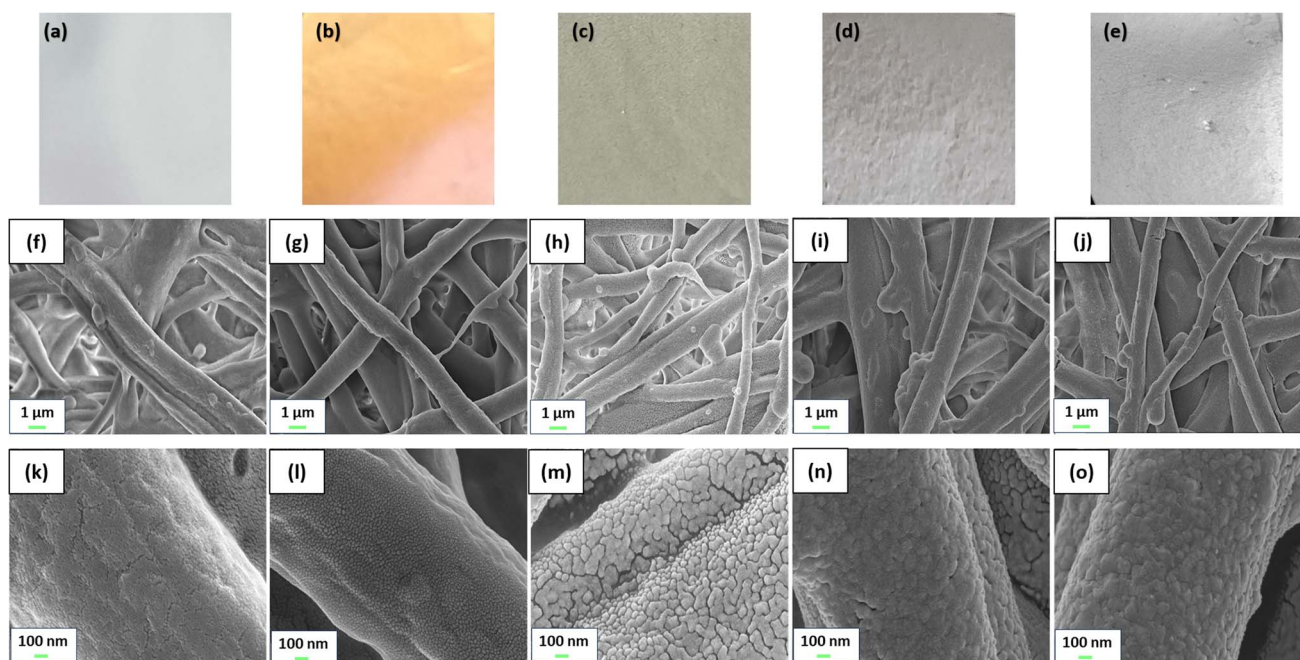

Fig. 4 Photographs of (a) natural ESM, (b) ESM/5Ag, (c) ESM/20Ag, (d) ESM/40Ag and (e) ESM/100Ag. FE-SEM images of (f and k) natural ESM, (g and l) ESM/5Ag, (h and m) ESM/20Ag, (i and n) ESM/40Ag and (j and o) ESM/100Ag.
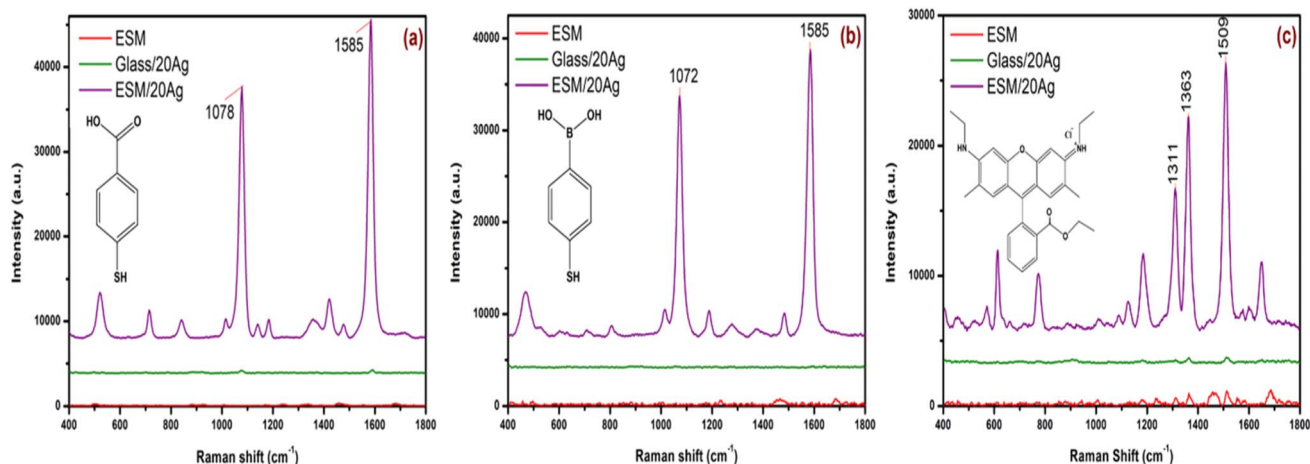
Fig. 5 Raman spectra of 1 mM (a) 4-MBA, (b) 4-MPBA and (c) R6G on ESM, Ag coated ESM and Ag coated glass (laser power 37 mW).

ability of ESM/20Ag (Fig. 4). The ESM/20Ag substrate has the most suitable Ag coating to generate electromagnetic hotspots compared to higher coating thicknesses that form a continuous silver film and reduce the hotspots for signal enhancement.[37]

Fig. 5a–c show the Raman spectra obtained when 1 mM solutions of 4-MBA, 4-MPBA and R6G, respectively, were drop cast onto bare ESM, ESM/20Ag as well as 20 nm Ag-coated glass slide (Glass/20Ag). The ESM/20Ag substrate generated sharp, well-defined peaks of all three analytes, demonstrating effective Raman signal enhancement. The 20 nm Ag-coated glass slide displayed Raman peaks for 4-MBA at 1585 and 1078 cm^{-1}, but their intensities were significantly lower than those observed on the ESM/20Ag substrate. In contrast, the bare ESM could not support any signal enhancement for either 4-MBA or 4-MPBA. Additionally, a 1 mM solution of R6G on bare ESM and the Ag-coated glass also exhibited a few Raman signals, but their intensities were very weak compared to those from the ESM/20Ag substrate (Fig. 5c).

Although the same thickness of silver was coated on both glass and ESM, the latter showed better signal amplification as ESM offers additional advantages for SERS enhancement. Deposition of Ag nanoparticles onto a 3D scaffold like ESM

enables the utilization of electromagnetic hotspots within the probe volume of the laser excitation.[38] Also, the inherent porous nature of the membrane can provide high-density hotspots owing to their large surface area, and the abundant functional groups present in ESM bestow anchoring sites for various analytes.[39] Furthermore, as a flexible platform, ESM overcomes the limitations of its rigid counterparts for real-life applications.

The surface enhancement factor (EF) for ESM/20Ag substrate was calculated using the following equation,[40]

$$EF = \frac{(I_{SERS}/N_{SERS})}{(I_{Normal}/N_{Normal})} \quad (1)$$

where I_{Normal} and I_{SERS} are the intensities for an identified peak obtained through conventional Raman and SERS measurements, respectively. N_{Normal} is the number of molecules probed for normal Raman scattering, and N_{SERS} is the number of molecules probed for SERS.

To determine EF for the fabricated substrate, intensities at 1078 cm^{-1} for 4-MBA, 1072 cm^{-1} for 4-MPBA, and 1509 cm^{-1} for R6G are considered. The EF values obtained for 1 mM solutions of 4-MBA, 4-MPBA and, R6G are 0.12×10^6, 0.70×10^5 and 0.36×10^4, respectively. Further details regarding the calculation of EF are provided in ESI.† To further evaluate the SERS ability of
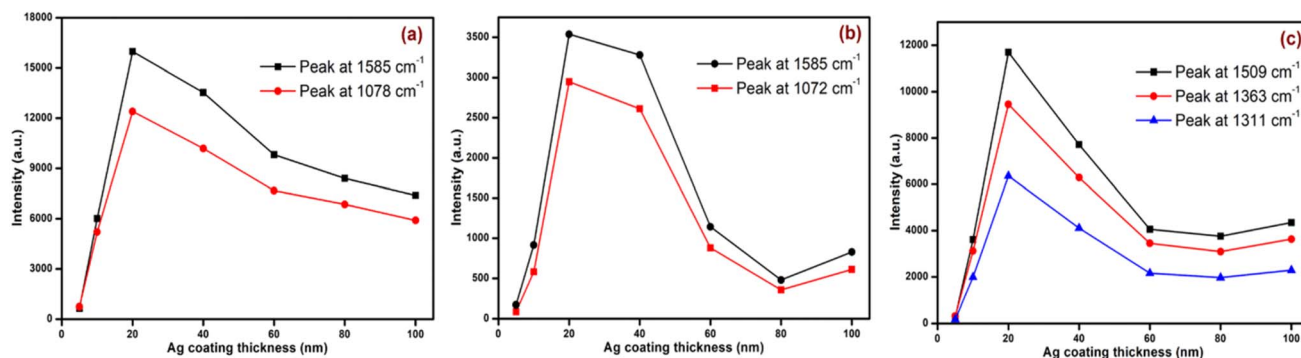

Fig. 6 Intensity variation of characteristic Raman peaks for (a) 4-MBA, (b) 4-MPBA and (c) R6G with change in Ag thickness of ESM/Ag substrates (laser power 11 mW, integration time 0.5 s).
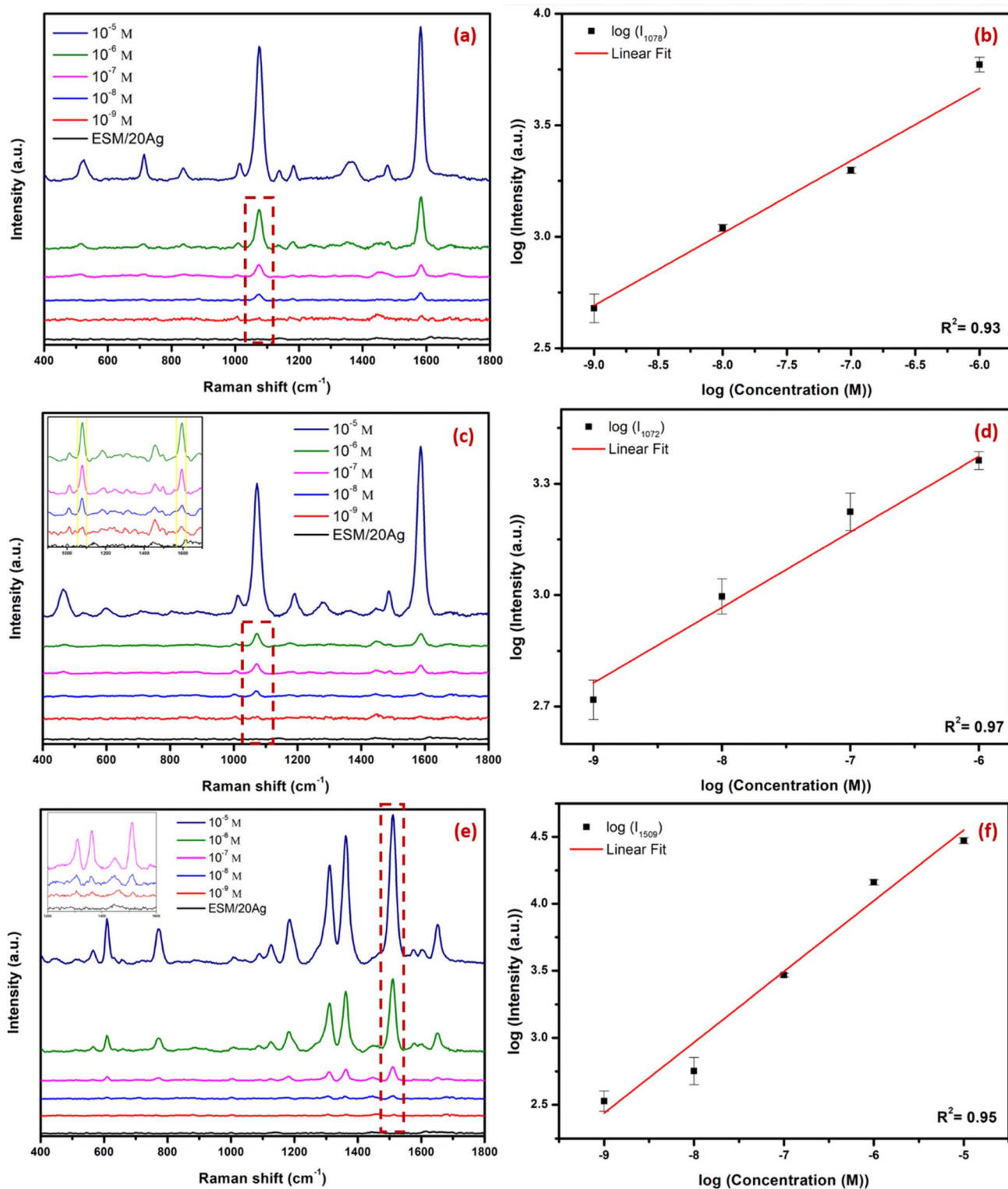
Fig. 7 Concentration dependent SERS spectra of (a) 4-MBA (c) 4-MPBA and (e) R6G on ESM/20Ag substrate. The linear relationship of logarithmic SERS intensity *versus* logarithmic concentration for (b) peak 1078 cm^{-1} of 4-MBA, (d) peak 1072 cm^{-1} of 4-MPBA and (f) peak 1509 cm^{-1} of R6G. Calibration curve error bar represents the standard deviation of three measurements.

the developed substrates, Raman spectra of varying concentrations (10 μM to 1 nM) of the analytes on ESM/20Ag were recorded. As shown in Fig. 7, the detectable peaks were obtained up to 10^{-9} M concentrations for 4-MBA, 4-MPBA and, R6G, confirming the SERS potential of the substrate. A linear relationship between the logarithmic SERS intensity and the
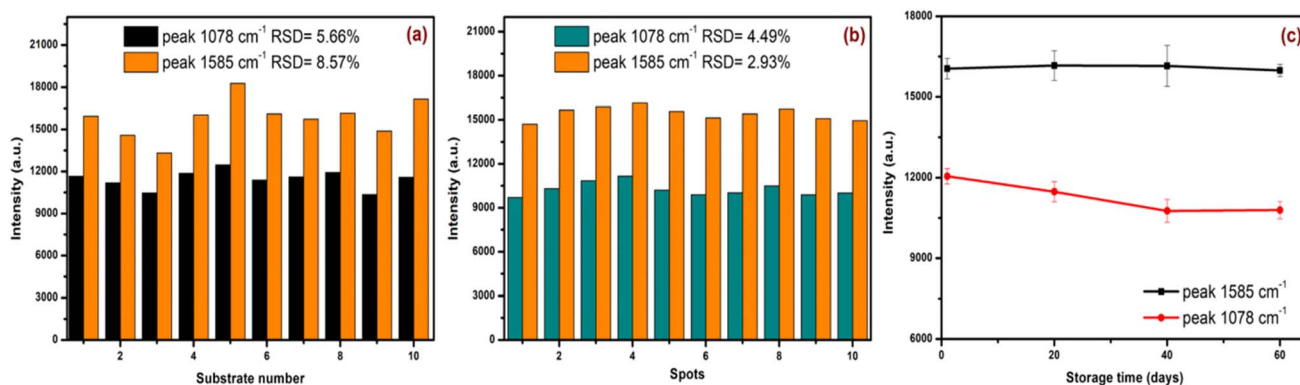
Fig. 8 Intensity variation of Raman peaks for 1 mM 4-MBA on ESM/20Ag substrate (a) ten different fabrication batches (b) ten different locations on a single substrate and (c) after 60 days storage at ambient conditions.

Table 1 Comparison of the ESM/20Ag SERS substrate with other reported SERS platforms ("—" indicates data not reported in the corresponding publication)

Substrate	Analyte	LOD	Reproducibility	Stability	Ref.
Ag films deposited on silicone oil	R6G	10^{-7} M	—	—	41
AgNPs on nickel foam	R6G	10^{-9} M	—	30 days	42
Ag on PDMS-replicated beetle-wing structure	R6G	10^{-6} M	—	—	43
Ag NPs on wrinkled PDMS film	R6G	10^{-7} M	7.3%	—	44
QSERS (Nanova Inc.)	4-MBA	8.7×10^{-6} M	—	—	45
RAM-SERS-SP (Ocean Optics)	4-MBA	1.1×10^{-5} M	—	—	
Hamamatsu (Hamamatsu Photonics)	4-MBA	8.2×10^{-6} M	—	—	
ESM/20Ag	R6G	10^{-9} M	5.6%	60 days	Our work
	4-MBA	10^{-9} M			
	4-MPBA	10^{-9} M			

logarithmic concentration was observed for the characteristic peaks of each analyte: the 1078 cm^{-1} peak of 4-MBA (Fig. 7b), the 1072 cm^{-1} peak of 4-MPBA (Fig. 7d) over the concentration range of 1 μM to 1 nM, and the 1509 cm^{-1} peak of R6G (Fig. 7f) from 10 μM to 1 nM. All the measurements were conducted under a laser power of 37 mW with an integration time of 10 seconds. The experiments were conducted using a portable handheld Raman instrument, showcasing the practical application of the developed ESM/20Ag substrate in portable, on-site analytical applications with reliable sensitivity.

3.4 Uniformity, stability and reproducibility of the ESM/Ag substrate

To develop a high-quality SERS substrate, it is necessary to consider good signal enhancement, the reproducibility of the fabrication process, uniformity, and stability of the substrates. These factors were evaluated by analyzing the variation in intensities of two characteristic peaks of 4-MBA at 1078 and 1585 cm^{-1} under identical measurement conditions, 11 mW laser power and 0.5 s integration time. The fabrication process was repeated ten times under similar conditions to obtain ESM/20Ag substrates using thermal evaporation. The SERS spectra of 4-MBA were measured on these ten different substrates to evaluate the reproducibility (Fig. 8a). The substrate fabrication process was reproducible with the intensity variations at 1078

and 1585 cm^{-1} for 4-MBA having a relative standard deviation (RSD) of 5.66% and 8.57%, respectively.

To determine the uniformity of the substrate, 1 mM 4-MBA solution was drop casted on ESM/20Ag substrate, and SERS spectra were recorded at ten randomly selected spots on the substrate under the same measurement conditions. Consistent Raman intensities obtained for peaks at 1078 and 1585 cm^{-1} with RSD of 4.49% and 2.93%, respectively, confirm the uniformity of the developed SERS substrate (Fig. 8b). The stability of the substrate stored in ambient conditions was determined by monitoring the 4-MBA signal intensities for 60 days. The substrate maintained relatively consistent SERS performance even after 60 days, as is clear from Fig. 8c. The high uniformity, good reproducibility, and excellent ESM/Ag substrate stability demonstrate its potential to exploit as a sensing platform for practical applications.

3.5 Performance comparison with existing SERS platforms

To comprehensively evaluate the performance of the proposed ESM/20Ag substrate, we compared it with other SERS substrates fabricated using thermal evaporation techniques as well as selected commercial SERS platforms. Table 1 summarizes the detection limits, reproducibility, and stability of ESM/20Ag substrate along with several recently reported SERS substrates.

The ESM/20Ag substrate achieved a low detection limit (LOD) of 10^{-9} M for R6G, 4-MBA, and 4-MPBA, with good reproducibility (5.6% RSD) and excellent signal stability over 60 days. These figures are comparable to or better than many SERS substrates made using thermal evaporation methods, such as Ag films on silicone oil or Ag on nickel foam surfaces. Furthermore, when compared to commercial SERS substrates (QSERS, RAM-SERS-SP, Hamamatsu), the ESM/20Ag substrate demonstrates significantly lower detection limit for 4-MBA and offers advantages in cost-effectiveness, biodegradability, and ease of fabrication. Unlike synthetic templates like wrinkled polydimethylsiloxane (PDMS) or bionic beetle-wing replicas, the bio-derived ESM requires no complex patterning while still achieving reliable SERS signals. These findings highlight the ESM/Ag as a promising, environmentally friendly, and scalable alternative for practical SERS applications.

4. Conclusions

The inexpensive eggshell membrane (ESM) waste material was successfully transformed into a potential cost-effective SERS active platform by Ag deposition using the thermal evaporation technique. The multi-dimensional nature and porosity of ESM endow a natural framework for high-density electromagnetic hotspots. The ESM substrate with a silver deposition of 20 nm thickness having suitably arranged hotspots exhibited remarkable SERS activity for standard Raman analytes such as, 4-MBA (EF = 0.12×10^6), 4-MPBA (EF = 0.70×10^5) and R6G (EF = 0.36×10^4). The as developed fabrication method is highly reproducible, and the resulting SERS substrate exhibited excellent uniformity as well as stability for up to 60 days at ambient storage conditions. The results demonstrate that the Ag coated ESM substrate can act as an effective and flexible sensing platform for the label-free detection of a wide variety of target molecules. Work is underway to demonstrate the potential of this prospective SERS substrate as a cost-effective platform for various molecular detection and diagnostic applications.

Data availability

All data has been presented in the manuscript and ESI.†

Author contributions

V.S. Swathy Lekshmy: Writing – original draft, conceptualization, investigation, methodology, validation. Subramee Sarkar: Methodology, validation. Karuvath Yoosaf: Software, writing – review and editing. Joshy Joseph: Supervision, writing – review and editing. P. Sujatha Devi: Conceptualization, supervision, writing – review and editing.

Conflicts of interest

There are no conflicts to declare.

Acknowledgements

References

1 X. Han and B. Zhao, in *Molecular and Laser Spectroscopy*, ed. V. P. Gupta and Y. Ozaki, Elsevier, 2020, pp. 349–386, DOI: **10.1016/b978-0-12-818870-5.00010-1**.

2 J. Langer, D. Jimenez de Aberasturi, J. Aizpurua, R. A. Alvarez-Puebla, B. Auguie, J. J. Baumberg, G. C. Bazan, S. E. J. Bell, A. Boisen, A. G. Brolo, J. Choo, D. Cialla-May, V. Deckert, L. Fabris, K. Faulds, F. J. Garcia de Abajo, R. Goodacre, D. Graham, A. J. Haes, C. L. Haynes, C. Huck, T. Itoh, M. Kall, J. Kneipp, N. A. Kotov, H. Kuang, E. C. Le Ru, H. K. Lee, J. F. Li, X. Y. Ling, S. A. Maier, T. Mayerhofer, M. Moskovits, K. Murakoshi, J. M. Nam, S. Nie, Y. Ozaki, I. Pastoriza-Santos, J. Perez-Juste, J. Popp, A. Pucci, S. Reich, B. Ren, G. C. Schatz, T. Shegai, S. Schlucker, L. L. Tay, K. G. Thomas, Z. Q. Tian, R. P. Van Duyne, T. Vo-Dinh, Y. Wang, K. A. Willets, C. Xu, H. Xu, Y. Xu, Y. S. Yamamoto, B. Zhao and L. M. Liz-Marzan, *ACS Nano*, 2020, **14**, 28–117.

3 C. L. Haynes, A. D. McFarland and R. P. Van Duyne, *Anal. Chem.*, 2005, **77**, 338A–346A.

4 H. Y. Wu, H. C. Lin, G. Y. Hung, C. S. Tu, T. Y. Liu, C. H. Hong, G. Yu and J. C. Hsu, *Nanomaterials*, 2022, **12**, 2742.

5 O. Peron, E. Rinnert, M. Lehaitre, P. Crassous and C. Compere, *Talanta*, 2009, **79**, 199–204.

6 X. Y. Ling, C. Acikgoz, I. Y. Phang, M. A. Hempenius, D. N. Reinhoudt, G. J. Vancso and J. Huskens, *Nanoscale*, 2010, **2**, 1455–1460.

7 M. Sajitha, B. Abraham, R. B. Nelliyil and K. Yoosaf, *ACS Appl. Nano Mater.*, 2021, **4**, 10038–10046.

8 S. Y. Chou, C. C. Yu, Y. T. Yen, K. T. Lin, H. L. Chen and W. F. Su, *Anal. Chem.*, 2015, **87**, 6017–6024.

9 B. B. Xu, Y. L. Zhang, W. Y. Zhang, X. Q. Liu, J. N. Wang, X. L. Zhang, D. D. Zhang, H. B. Jiang, R. Zhang and H. B. Sun, *Adv. Opt. Mater.*, 2013, **1**, 56–60.

10 N. L. Garrett, P. Vukusic, F. Ogrin, E. Sirotkin, C. P. Winlove and J. Moger, *J. Biophotonics*, 2009, **2**, 157–166.

11 Z. Mu, X. Zhao, Z. Xie, Y. Zhao, Q. Zhong, L. Bo and Z. Gu, *J. Mater. Chem. B*, 2013, **1**, 1607–1613.

12 I. Tanahashi and Y. Harada, *J. Mater. Chem. C*, 2015, **3**, 5721–5726.

13 J. L. Arias, M. S. Fernandez, J. E. Dennis and A. I. Caplan, *Connect. Tissue Res.*, 1991, **26**, 37–45.

14 M. Wong, M. J. Hendrix, K. von der Mark, C. Little and R. Stern, *Dev. Biol.*, 1984, **104**, 28–36.

15 P. S. Devi, S. Banerjee, S. R. Chowdhury and G. S. Kumar, *RSC Adv.*, 2012, **2**, 11578–11585.

16 Q. Wang, C. Ma, J. Tang, C. Zhang and L. Ma, *Nanoscale Res. Lett.*, 2018, **13**, 255.

17 S. Pramanik, S. Chatterjee, G. Suresh Kumar and P. Sujatha Devi, *Phys. Chem. Chem. Phys.*, 2018, **20**, 20476–20488.

18 S. Ishikawa, K. Suyama, K. Arihara and M. Itoh, *Bioresour. Technol.*, 2002, **81**, 201–206.

19 N. Liu, Y. N. Liu, Y. S. Luan and X. J. Hu, *Appl. Mech. Mater.*, 2013, **299**, 207–210.

20 S. Pramanik, A. Saha and P. S. Devi, *RSC Adv.*, 2015, **5**, 33946–33954.

21 B. Li, D. Lan and Z. Zhang, *Anal. Biochem.*, 2008, **374**, 64–70.

22 B. Zheng, S. Xie, L. Qian, H. Yuan, D. Xiao and M. M. F. Choi, *Sens. Actuators, B*, 2011, **152**, 49–55.

23 P. Y. Lin, C. W. Hsieh, P. C. Tsai and S. Hsieh, *ChemPhysChem*, 2014, **15**, 1577–1580.

24 Y. Li, Y. Ye, Y. Fan, J. Zhou, L. Jia, B. Tang and X. Wang, *Crystals*, 2017, **7**, 45.

25 Q. Ding, Z. Kang, X. He, M. Wang, M. Lin, H. Lin and D. P. Yang, *Microchim. Acta*, 2019, **186**, 453.

26 Q. He, D. Wang, J. Shao, Y. Li, M. Cheng, L. Dong, Y. Li, J. Zhu and H. Li, *J. Mol. Struct.*, 2023, **1289**, 135883.

27 D. J. Semin and K. L. Rowlen, *Anal. Chem.*, 1994, **66**, 4324–4331.

28 B. T. Scarpitti, A. M. Morrison, M. Buyanova and Z. D. Schultz, *Appl. Spectrosc.*, 2020, **74**, 1423–1432.

29 D. Gao, X. Yang, M. Luo, P. Teng, H. Zhang, Z. Liu, S. Gao, Z. Li, X. Wen, L. Yuan, K. Li, M. Bowkett and N. Copner, *ACS Appl. Nano Mater.*, 2021, **4**, 10784–10790.

30 M. M. Hassan, W. Ahmad, M. Zareef, Y. Rong, Y. Xu, T. Jiao, P. He, H. Li and Q. Chen, *Food Chem.*, 2021, **358**, 129844.

31 T. M. James, M. Schlosser, R. J. Lewis, S. Fischer, B. Bornschein and H. H. Telle, *Appl. Spectrosc.*, 2013, **67**, 949–959.

32 N. Wang, Z. Ma, S. Zhou and G. Liang, *Chem. Phys. Lett.*, 2016, **666**, 45–50.

33 M. C. Yang, T. Y. Chien, Y. W. Cheng, C. K. Hsieh, W. L. Syu, K. S. Wang, Y. C. Chen, J. S. Chen, C. C. Chen and T. Y. Liu, *Spectrochim. Acta, Part A*, 2023, **303**, 123190.

34 L. Jiang, T. You, P. Yin, Y. Shang, D. Zhang, L. Guo and S. Yang, *Nanoscale*, 2013, **5**, 2784–2789.

35 S. Li, Q. Zhou, W. Chu, W. Zhao and J. Zheng, *Phys. Chem. Chem. Phys.*, 2015, **17**, 17638–17645.

36 X. N. He, Y. Gao, M. Mahjouri-Samani, P. N. Black, J. Allen, M. Mitchell, W. Xiong, Y. S. Zhou, L. Jiang and Y. F. Lu, *Nanotechnology*, 2012, **23**, 205702.

37 J. Perumal, K. V. Kong, U. S. Dinish, R. M. Bakker and M. Olivo, *RSC Adv.*, 2014, **4**, 12995–13000.

38 W. Hu, L. Xia, Y. Hu and G. Li, *Microchem. J.*, 2022, **172**, 106908.

39 M. Balaz, *Acta Biomater.*, 2014, **10**, 3827–3843.

40 B. Abraham, N. Emmanuel, N. Ajikumar, S. Pulassery, L. E. Varghese, V. P. Murali, A. Munnilath, K. K. Maiti and K. Yoosaf, *ChemNanoMat*, 2023, **9**, e202300378.

41 G. Sun, G. Ye, K. Wang, M. Lou, X. Jia, F. Xu and Z. Ye, *ACS Omega*, 2020, **5**, 7440–7445.

42 Z. Zhou, A. Xie, Y. Tan, J. Zhang and C. Xue, *New J. Chem.*, 2023, **47**, 21225–21231.

43 C. H. Lu, M. R. Cheng, S. Chen, W. L. Syu, M. Y. Chien, K. S. Wang, J. S. Chen, P. H. Lee and T. Y. Liu, *Polymers*, 2022, **15**, 191.

44 H. Zhang, Z. Zhang, H. Wang, L. Huang, Z. Yang, Y. Wang and H. Li, *Opt. Express*, 2023, **31**, 21025–21037.

45 A. Azziz, W. Safar, Y. Xiang, M. Edely and M. Lamy de la Chapelle, *J. Mol. Struct.*, 2022, **1248**, 131519.